Non-Invasive Estimation of Subcutaneous and Visceral Adipose Tissue Blood Flow by Using [^{15}O]H_2O PET with Image Derived Input Functions

Kaisa E. Liukko[1], Vesa J. Oikonen[1], Tuula K. Tolvanen[1], Kirsi A. Virtanen[1], Antti P. Viljanen[1], Hannu T. Sipilä[1], Pirjo Nuutila[1] and Patricia Iozzo[*,1,2]

[1]*Turku PET Centre, University of Turku, FI 20521, Turku, Finland*

[2]*Institute of Clinical Physiology, National Research Council, 56100 Pisa, Italy*

Abstract: Subcutaneous adipose tissue blood flow is finely regulated, and tuned with fat metabolism; little is known about visceral fat, which is less accessible in humans. In estimating blood flow with positron emission tomography (PET) and oxygen-15-labelled water ([^{15}O]H_2O), the input function is obtained invasively from arterial blood samples. The aim of the current study was to validate a non-invasive method to measure blood flow in adipose depots, by extracting input function curves from [^{15}O]H_2O-PET images. Data of twenty subjects undergoing abdominal [^{15}O]H_2O-PET were used. Images were reconstructed with filtered backprojection (FBP). Location, diameter, and inner radioactivity levels of the abdominal aorta were automatically determined. Image derived arterial curves (IDI) were compared to measured arterial blood data, as obtained by an online blood sampler (OSI). Blood flow in three adipose tissue depots was estimated using the autoradiographic method with OSI *vs* the FBP image derived input (F-IDI) function. Correlations between blood flow results obtained with OSI and IDI were significant ($r \geq 0.87$, $p < 0.0001$) in all regions. Estimates of the aortic diameter ranged between 10.7-17.2 mm. A good agreement was found between area under the curve (AUC) values of F-IDI and OSI curves; the $AUC_{F\text{-}IDI}/AUC_{OSI}$ ratio was 0.97±0.10. Our results support the implementation of the current method for the non-invasive detection of the abdominal aorta input function from a dynamic [^{15}O]H_2O PET image in the quantification of regional blood flow in low flow tissues. This method allows simultaneously examine subcutaneous and intra-abdominal fat depots.

INTRODUCTION

Adipose tissue blood supply and metabolism are tightly coordinated [1-3], and the modulation of adipose tissue blood flow appears necessary to both remove free fatty acid away from, and deliver lipoproteins to the tissue, depending on the nutritional state [4]. Abnormalities in the regulation of this process seem to be a feature of insulin resistance and obesity and they are focus of intense investigation [5-7]. The assessment of blood flow by xenon washout rates or microdialysis [8] has been fundamental in the understanding of adipose tissue (patho)physiology, but is confined to subcutaneous fat. Visceral fat has been closely related with metabolic risk, insulin resistance, and liver metabolism [9,10], and is inaccessible with the above procedures in humans *in vivo*. We have recently adopted Positron Emission Tomography (PET) and oxygen-15 labeled water ([^{15}O]H_2O) in the quantification of adipose tissue blood flow, and our initial evaluation demonstrates that the impairment of blood flow during insulin stimulation involves visceral fat in obese individuals [11]. Unfortunately, some degree of invasiveness is associated with this technique, since the estimation of regional blood flow by dynamic PET imaging requires that arterial radioactivity concentrations (input function) are measured, which is challenging, and not always successful, especially in obese individuals. The new design of combined PET/CT scanners makes it further complicated to reach the sampling site, given a deep gantry.

*Address correspondence to this author at the Institute of Clinical Physiology, National Research Council, 56100 Pisa, Italy;
E-mail: patricia.iozzo@ifc.cnr.it

Methods to derive arterial time-activity curves (TACs) directly from a PET image have been suggested [12-25]. Independent Component Analysis based methods (EPICA – extraction of the plasma TAC using Independent Component Analysis) have been used to obtain input curves from [^{18}F]FDG and [^{11}C]MPDX human brain data [12,13]. The disadvantage of this method is that one arterial blood sample is needed if quantitative results are required.

A region of interest (ROI) based input extraction, in which an operator manually delineates vascular areas in the image and radioactivity levels are extracted from the defined location, has been used for the carotid artery [14], abdominal artery [15], different myocardial cavities and segments of the thoracic aorta [16, 23, 25]. In these approaches, the partial volume effect – i.e., the underestimation of radioactivity levels caused by a vessel diameter that is in the same range as scan resolution - has been taken into account, by testing different ROI sizes or thresholding the pixels inside arterial ROIs. Manual ROI drawing is operator and ROI-size dependent, and it necessitates that partial volume correction is considered separately in each ROI.

A relatively automatic image derivation method without ROI drawing was applied to filtered backprojection (FBP)-reconstructed [^{15}O]H_2O PET studies in human and canine models [17]. This method automatically finds the abdominal aorta from a PET image and determines the un-recovered input curve from 2-3 mm regions, i.e., less than 1/5 of the vessel diameter, closest to the pixel with maximal activity. A recovery coefficient accounting for the spatial resolution of the image and for the radius of the aorta is needed to correct radioactivity concentrations. In the above study, the diameter

1874-3471/07

of the aorta was estimated from the image by fitting a radioactivity profile function into image planes containing the vessel.

The current study was undertaken to optimise and validate the extraction of an arterial $[^{15}O]H_2O$ input function from PET images including the abdominal aorta in humans, by using recovery coefficient and radioactivity profile model [17]. The model estimates the diameter of the aorta and is fitted to the two-dimensional image matrix surrounding the vessel and adjusted to take into account the radioactivity in the surrounding tissues [19]. In addition to FBP-reconstructed images, the method was validated for images reconstructed with Bayesian iterative algorithm using median root prior (MRP) filter. Image derived TACs (IDI) were compared with those measured with an online blood sampler (OSI TACs) and both were used to estimate blood flow in three adipose tissue depots.

MATERIALS AND METHODS

Dynamic PET Scanning

A full data set of twenty human subjects, including 10 lean and 10 obese subjects, was used to validate our input curve extraction method. The current data were acquired as part of an investigation around obesity and adipose tissue metabolism and blood flow, as previously reported [11]. Subjects were of 25-40 years of age, healthy and not taking any medication. The protocol was approved by the Ethical Committee of Turku University Hospital.

An ECAT 931/08 tomograph (CTI/Siemens, Knoxville, TN), with 15 planes, slice width of 6.75 mm and pixel size of 4.69 mm, was used. Two catheters were inserted, one in a left antecubital vein for injection of $[^{15}O]H_2O$, and the other in the right radial artery for blood sampling. After injection of 1.2-1.3 GBq of $[^{15}O]H_2O$, a dynamic scan of the abdominal region was performed for 6 min (6x5sec, 6x15sec and 8x30sec). Online blood sampling (Scanditronix, Uppsala, Sweden) at a rate of 6 ml/min was simultaneously carried out with one-second framing. The online sampler consisted of two pairs of coincidence BGO crystals and a peristaltic pump. The detectors had been cross-calibrated to the PET scanner *via* ion chamber. The blood curve from the online sampler was calibrated and corrected for decay and dispersion [26]. Dispersion constant 5.0 was used for correction of physiological dispersion and 2.5 for correction of tube dispersion.

Delay corrections were done against the average curves of adipose tissue regions. The delay correction is based on methods developed by Meyer [27] and van den Hoff *et al.* [28], in which the blood curve is shifted with different delay times and a three-compartment model with parameters K1-K4 and Vb is fitted to the data. The curve that fits best is determined by finding the lowest sum-of-squares value and the estimate for delay is chosen accordingly.

Two reconstruction methods were applied to all twenty images, 1) filtered backprojection (FBP) using Hann filter and cutoff 0.5, and 2) Bayesian iterative algorithm using median root prior (MRP) with 150 iterations and the Bayesian coefficient of β=0.3. The spatial resolution of 10 mm full width at half maximum (FWHM) at the centre of the image was assumed for both FBP and MRP. This value has previously been reported for FBP reconstructed images [29]. For MRP a value of 7.8 mm FWHM at the centre of the field of view has been published [29], but was slightly lower than optimal for our data, probably due to the relatively small size of the aorta, and its non-central location.

Anatomical reference images of the abdominal area were acquired with a 0.23 T Outlook GP (Marconi Medical Systems Inc., Cleveland, OH) magnetic resonance scanner. ROIs in subcutaneous, visceral and perirenal regions were drawn on MRI images and copied to the $[^{15}O]H_2O$ PET images to obtain tissue TACs, as previously described [11].

Input Curve Extraction

A threshold method was used to find the aorta in dynamic PET-images. Suitable planes were selected visually from the image, since the abdominal aorta is clearly distinguishable in the first half of $[^{15}O]H_2O$ image time frames, as facilitated by a vessel diameter of approximately 15-20 mm, and negligible radioactivity in the background. The maximum radioactivity concentration immediately after intravenous injection of $[^{15}O]H_2O$ was assumed to result from blood. Pixels in the same area, with radioactivity concentrations >85% of the maximum observed in each early frame, were considered to be in the vessel. The radioactivity concentration in blood was then calculated in each frame as the mean value in these pixels.

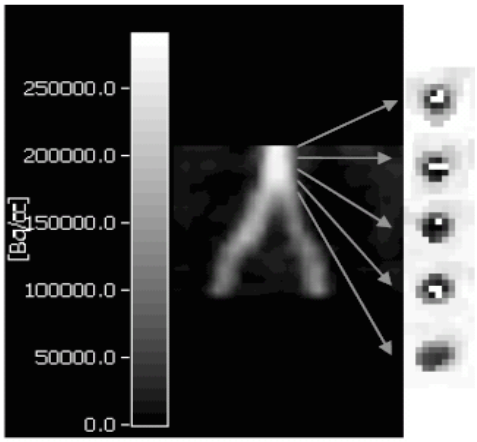

Fig. (1). *Left panel*: coronal view of subject 2 (frame 7) showing the abdominal aorta. *Right panel*: transaxial view showing five cross-sections of the aorta; the selected pixels are highlighted in white.

In detail, the threshold algorithm was implemented as follows. In transaxial PET images, 3 to 8 planes were chosen in which the aorta could be visualized, as a single round area (Fig. **1**). Then, the pixel with maximum radioactivity concentration $c_{PET}(x_{max}, y_{max}, z_{max}, f_{max})$ was searched across all frames and the selected planes, and assigned to blood if the integrated area (AUC) of its time-activity curve at 0-3 min was larger than that at 3-6 min. After identifying one pixel in the abdominal aorta, an axial bar-shaped portion of the image, including adjacent pixels, was isolated to form a separate dynamic image. The image was created with the maximum pixel at the centre of 30×30 mm transaxial planes and it included the 3-8 planes selected at the start of the procedure (Fig. **1**). The original framing was preserved. Then all pixels in the frame f_{max} with radioactivity concentration greater than $0.85 \times c_{PET}(x_{max}, y_{max}, z_{max}, f_{max})$ were selected.

Radioactivity concentrations in all selected pixels, including the one with maximum concentration, were averaged for each frame.

A recovery coefficient [17] is needed to correct the image-derived blood time-activity curve for partial volume and spill-over effects, caused by the limited spatial resolution of PET. The level of correction depends on the radius of the abdominal aorta and the spatial resolution of the image. The radius of the aorta was estimated by a modified model. The bar-shaped image - as described above - was used to fit the model on plane z_{max}. The equation describing the radioactivity profile *c(x,y)* in the plane was:

$$c(x,y) = c_{bg} + \frac{A}{2} ERF\left(\frac{\sqrt{(x-x_{mid})^2 + (y-y_{mid})^2} + R}{s\sqrt{2}} \right) - \frac{A}{2} ERF\left(\frac{\sqrt{(x-x_{mid})^2 + (y-y_{mid})^2} - R}{s\sqrt{2}} \right)$$

where $s = \frac{FWHM}{2\sqrt{2\ln(2)}}$, $A = c_{iv} - c_{bg,}$

x_{mid} and y_{mid} are the coordinates of the centre of the aorta, R is the radius of the vessel, c_{iv} represents the radioactivity concentration inside the vessel and c_{bg} is the background radioactivity concentration. Because c_{bg} was fitted to be constant throughout the image, c_{iv} was the sum of the estimated A and c_{bg}. ERF is the error function encountered in integrating the normal distribution. It is defined as:

$$ERF(x) = \frac{2}{\sqrt{\pi}} \int_0^x e^{-t^2} dt$$

All five parameters, x_{mid}, y_{mid}, c_{bg}, A and R were fitted to the non-weighted bar-shaped PET image data. The Powell-Brent algorithm [30] was used, which optimises model parameters based on least squares evaluation between modelled *c(x,y)* and observed $c_{PET}(x,y)$ radioactivity values. The radius R was estimated from the fit on frame f_{max}. Background c_{bg} was estimates in all frames but at that point the parameters x_{mid}, y_{mid} and R were fixed based on the first fit. The radioactivity concentration c_{iv}(t) was used only for estimation of R, and not to construct the final arterial curve.

Then, RC was calculated as [17]:

$$RC = 1 - e^{-\frac{R^2}{2s^2}}$$

For FBP data the spatial resolution value measured in the centre of the field of view (FOV) was used, best approximating the quasi-central location of the abdominal aorta in the image and FOV. In case of MRP data, the measured spatial resolution value (7.8 mm, centre of the field of view) led to overestimation of blood flow and thus different values were experimented. Spatial resolution of 10 mm FWHM was found to give the best estimates for the blood flow results.

Finally, the arterial blood curve was computed by using the following formula [19]:

$$c_{arterial}(t) = c_{bg}(t) + \frac{1}{RC}(c_{threshold}(t) - c_{bg}(t))$$

The timing of the resulting TAC was corrected against the average adipose tissue TAC to cross-match the initial rise in radioactivity concentrations.

The curves obtained from the image were compared with the measured arterial TACs. Then, both arterial curves were used to estimate blood flow in adipose tissue with the autoradiographic method [26] using partition coefficient 0.19. A period of 250 seconds was used in blood flow analysis and the starting time point was determined individually for each subject from visualizations of arterial TACs.

Statistical Analysis

IDI curves were validated by comparing the areas under the curve (AUC) to those obtained from OSI curves and by runs test comparison [31]. For runs test comparisons, the OSI curves were reframed to match the frames of the image. Runs test method detects nonrandomness of residuals between two curves based on number of runs between the curves, when a run is defined as a subsequence of residuals having the same sign. Too few runs indicate that the two curves are not likely to be the same. Whereas AUC comparison verifies that the level of radioactivity is the same throughout the period of 250 sec, the runs test will reveal us if the shapes of the curves are not likely to be the same at the level of significance p less than 0.05.

Blood flow results are shown as mean±SD. The Student's paired t test and Bland-Altman plots [32] were used to compare results of the image derived *vs* online sampler input function. Regression analyses were carried out by standard methods. A p value <0.05 was considered as statistically significant.

Software

The profile fitting method and runs test are implemented in ANSI C open source (GNU Lesser General Public License) programs (www.pet.fi, versions eabaort 1.4.1 and dftrunst 1.0.0). Statistical analysis was done with Microsoft Excel 10 and Origin 7.5.

RESULTS

Blood flow estimates from FBP reconstructed (F) images and F-IDI or OSI functions were strongly correlated (0.94, 0.87 and 0.97) in subcutaneous, perirenal and visceral adipose depots, respectively, as shown in Fig. (**2**). By using F-IDI, average blood flow values were 6.46±5.74, 7.13±4.80, and 7.48±6.32 mL blood/(100 mL tissue*min), as compared with 5.95±5.78, 6.28±3.92, and 7.10±7.02 mL blood/(100 mL tissue*min) with OSI curves, in subcutaneous, perirenal and visceral fat, respectively (non-significantly different from F-IDI). Bland-Altman comparisons showed a good equivalence between blood flow values obtained with the two methods, with average differences (between blood flow estimates, proportional to the mean of the two estimates) of 10±24% (FBP) in subcutaneous, 10±25% in perirenal and 9±21% in visceral areas. These figures indicate an approximate 9% non-significant overestimation of blood flow by F-IDI *vs* OSI.

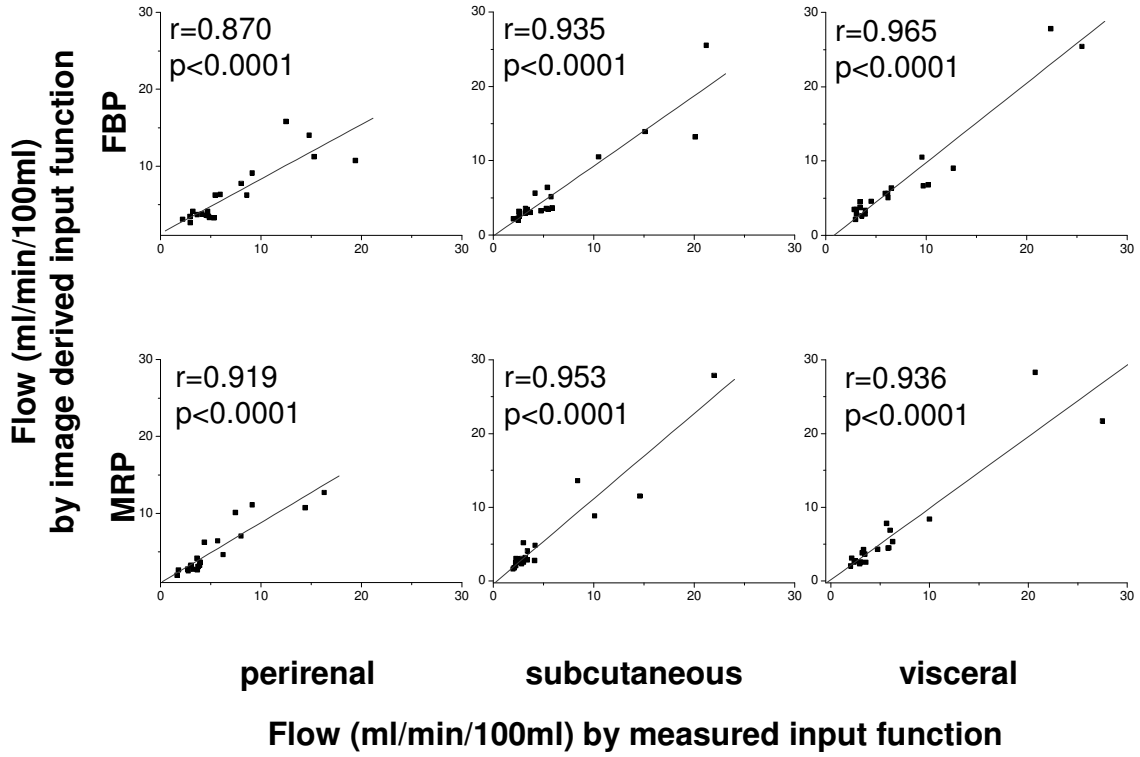

Fig. (2). Regression analysis, showing an excellent correlation between perfusion values calculated with the measured (*x-axis*) *vs* the estimated input function (*y-axis*) in three adipose tissue regions.

In the case of MRP (M) data, no over- or underestimation between MRP image derived (M-IDI) and OSI derived adipose tissue blood flow was observed; thus, blood flow values estimated with M-IDI were on average 13% lower than the ones obtained with F-IDI (ns).

For the extraction of input curve, three to eight planes were selected as designed in all but one subject, in whom the aorta was clearly distinguishable in 13 planes. Examples of online sampler (OSI) blood input curve and image derived curves from FBP image (F-IDI) and MRP image (M-IDI) are plotted in Fig. (**3**), showing almost super-imposable radioactivity concentrations throughout the whole scanning period. Altogether, on average 10 pixels were identified in the thresholding procedure. Estimates of the aortic diameter ranged between 10.7-17.2 mm (Table **1**). The recovery correction for the image derived blood TAC was on average 30% for FBP images and 42% for MRP images (Table **1**). The AUC_{IDI}/AUC_{OSI} ratios were on average 0.97±0.10 and 1.21±0.16 for recovery corrected F-IDI and M-IDI, respectively (Table **1**). Runs test comparison between IDI curves *vs* OSI (Table **1**) revealed less differences between F-IDI *vs* OSI compared to M-IDI *vs* OSI. The shapes of the curves looked similar at visual inspection. Statistical comparison of F-IDI and M-IDI curve shapes revealed differences for 6 of the 20 subjects. In these cases, minimal differences in the level of activity values occurred. Both AUC and runs test comparisons were calculated for 250 seconds, i.e. the part of the curve that was also used in blood flow analysis.

DISCUSSION

Aim of this study was to verify the quality of blood flow estimates obtained with a non-invasive input curve extraction method designed to account for partial volume effects and background radioactivity. The present method has the advantages of being user-independent, reproducible and fast. As compared to other image derived estimations, the current one is further simplified, requiring only the dynamic PET image and the spatial resolution in the centre of the image. The method thresholds the arterial input curve and then recovers it from partial volume without needing any user interference. It does not require any blood sampling or ROI drawing.

The most important finding in the current study was that the comparison between the estimated and online sampled input function curves showed a good correspondence for FBP data, and equivalent accuracy in the estimation of blood flow, as confirmed by Bland-Altman analysis and by the tight correlation in blood flow results in each of the examined tissue regions. Adipose tissue blood flow can therefore be determined non-invasively.

Altogether, our results support the use of the current method in the quantification of blood flow in regions with relatively low blood flow, likely including skeletal muscles beside adipose tissue, and hold promise that the same basic principles could be adapted to high flow conditions. The investigation of blood flow in low flow regions has provided

Table 1. Estimated Aortic Parameters in Individual Study Subjects°

Subject	AUCidi/AUCosi		Runs Test (idi *vs* osi)		1/RC		Diameter (mm)		AUCidi/AUCidi (MRP/FBP)	Runs Test (F-idi *vs* M-idi)
	FBP	MRP	FBP	MRP	FBP	MRP	FBP	MRP		
1	0.880	1.071	+	+	1.30	1.40	14.60	13.40	0.98	-
2	0.894	1.169	+	-	1.26	1.43	15.00	13.10	1.08	+
3	0.960	1.267	+	+	1.33	1.48	14.20	12.80	1.06	+
4	1.138	1.245	-	+	1.36	1.45	13.90	13.00	0.90	-
5	0.992	1.107	+	-	1.37	1.40	13.70	13.40	0.87	+
6	0.832	1.056	-	-	1.25	1.40	15.20	13.50	1.03	+
7	0.947	1.087	+	-	1.25	1.32	15.30	14.30	0.98	+
8	0.813	1.210	+	-	1.22	1.42	15.70	13.30	1.15	+
9	0.930	1.084	+	-	1.24	1.26	15.40	15.00	0.94	-
10	0.789	1.156	-	-	1.15	1.30	17.20	14.50	1.12	+
11	1.004	1.118	+	+	1.37	1.44	13.70	13.10	0.94	-
12	1.096	1.234	+	+	1.32	1.36	14.30	13.90	0.99	+
13	1.127	1.342	+	+	1.50	1.82	12.60	10.70	0.94	-
14	0.875	0.969	-	-	1.24	1.32	15.40	14.30	0.91	+
15	0.990	1.419	+	+	1.21	1.39	15.80	13.50	1.19	+
16	1.056	1.099	+	-	1.39	1.35	13.50	14.00	0.81	+
17	1.030	1.316	+	-	1.20	1.28	16.00	14.80	0.99	+
18	1.071	1.627	+	+	1.33	1.62	14.20	11.80	1.18	-
19	1.061	1.514	+	-	1.28	1.45	14.80	13.00	1.10	-
20	0.955	1.290	+	+	1.33	1.51	14.20	12.50	1.13	+
Mean ± sd Correlation	0.972 ± 0.103	1.219 ± 0.165	16/20	9/20	1.30 ± 0.08	1.42 ± 0.13	14.7 ± 1.06	13.4 ± 1.01	1.014 ± 0.108	14/20
					0.717600933		0.673901273			

°RC = recovery coefficient, AUC = area under the curve from 0 to 250 secs, IDI = image derived input function, OSI = measured input function. Pearson's correlation coefficient represents correlation between FBP and MRP images. Runs test results are marked with "-" if a significant difference was found between curve shapes and "+" if not.

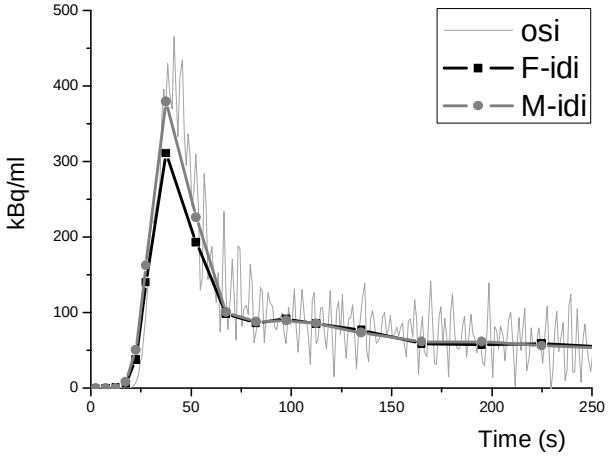

Fig. (3). Example of blood time-activity curves, showing the correspondence between online sampled (*light gray line*) and image estimated (*black line with squares and gray line with circles*) figures. The higher level of noise in the measured data is accounted for by dispersion correction.

important information on the pathogenesis of metabolic disorders, in which adipose tissue and skeletal muscle play an important causal role [33,34]. The possibility to avoid invasive arterial catheterisation procedures in this context is especially important, since patients bearing metabolic diseases are often overweight, making their vessels difficult to access, and they represent one major population target in investigations involving adipose tissue physiology. More than in other tissues, blood flow in subcutaneous fat appears to be finely modulated, and tuned with metabolic processes [5-7]; very little is known about nutrient and hormonal responses of visceral fat, in spite of the causal implication of this organ in the deterioration of the metabolic risk [9,10]. As compared with alternative methods to quantify adipose tissue blood flow, the current one adds the possibility to simultaneously explore - in a fully non-invasive fashion - several fat depots, including the intra-abdominal ones, which are otherwise inaccessible in human studies. The rapid radioactive decay of $[^{15}O]H_2O$ will make it possible to perform repeated measurements or to additionally image the metabolism of adipose tissue in corresponding areas during the same session, obtaining integrated information.

In most of the subjects, 3 to 8 PET image planes including the aorta were chosen based on visual detection. As an

exception, in subject number 6 the aorta seemed clearly distinguishable in 13 planes and they were all chosen. On average, the thresholding procedure selected 10 pixels (from all the planes) to describe arterial time activity. We obtained estimates of the diameter of the aorta in the range of 10.7-17.2 mm. Average values of 20 mm to 23 mm have been reported, depending on the aortic segment (suprarenal, infrarenal or maximal infrarenal) [35]. Since our method determines the internal diameter of the vessel, its value is expectedly slightly smaller than the published ones, which also include the vessel wall thickness [35]. In the current analysis, the diameter estimate was fitted for the plane in which the maximum radioactivity value was found. Planes that contained lower vessel radioactivity values provided higher estimates, as they are affected by the partial volume effect to a greater extent, and the recovery correction was not able to optimally balance for this error. The diameter estimation was in line with the expectations, it allowed us to obtain input curves overlapping the measured ones, and to quantify tissue blood flow with the same level of accuracy as with online sampler input; the comparison with anatomical images of reference will refine the computation of the aortic radius. In this study the resolution of anatomic images was not accurate enough for estimation of the diameter.

Since the profile fitting method includes the variable C (true activity inside the vessel), one may question why the latter was not used. The values of C and background activity are modeled for each frame, but the modeling of C becomes problematic in later frames of the image, when the background activity is dominant. For these frames, the modeled values for C can only be considered as an approximation, whereas a more accurate estimation is obtained by extracting true pixels and recovering the activity, as detailed here.

The theory of the method was originally based on FBP reconstruction [17], and our results show that the current method is not directly applicable to MRP data by using the published value of FWHM [29]. However, it was possible to empirically define a modified FWHM which provided comparable IDI and blood flow values, with non-statistically significant differences in the mean values compared with the gold-standard method, i.e., the use of measured radioactivity concentrations in arterial blood samples as input function. This modified FWHM needs to be separately determined for different scanners or reconstruction parameters.

In the literature, the effects of different ROI sizes, patient movement during scanning, partial volume effect and operator influence on ROI definition is reported [15,22]. EPICA was found to be a promising tool for non-invasive input extraction in [^{18}F]FDG and [^{11}C]MPDX studies [12]. However, the ICA only deals with relative radioactivity values, while absolute figures are lost in the process. This is not a problem if the target is to assess binding potentials, which can be calculated from relative values of distribution volumes (DV). But in the absolute quantification of DV or influx constants, one still needs to collect a blood sample.

Asselin *et al.* [24] have implemented a similar model fitting approach and obtained promising image derived input functions for 6-[^{18}F]fluoro-L-DOPA brain studies. Their model can to some extent take into account the heterogeneity of the background area. It is nonlinear in radius and centroid parameters, but linear in radioactivity concentration parameters, allowing use of the basis function method to fit the model. They reported that the bias for modeled radioactivity concentration is higher when the radioactivity is high, whereas in our hands the bias was detected in the late frames.

In studies requiring [11C]CO or [15O]CO scan to determine the blood volume, the estimation of the vessel diameter can be done with reduced bias from the CO image [18]. The current study supports the conclusion that input curves can be derived with sufficient accuracy without the additional CO scan.

The current method for abdominal aorta is simple and provides absolute determinations and operator independency in the assessment of blood flow. It forms the basis for further development, for example by using cluster analysis in place of thresholding, though the latter has the advantage of simplicity.

CONCLUSION

In conclusion, our results support the implementation of the current method for the non-invasive detection of the abdominal aorta input function from a dynamic [^{15}O]H_2O PET image in the quantification of regional blood flow in low flow tissues, allowing simultaneously examine subcutaneous and intra-abdominal fat depots in humans.

ACKNOWLEDGEMENTS

The study was financially supported by the Academy of Finland (2063509 to PN), Finnish Diabetes Foundation (2004 and 2005 to PI), EFSD/Eli-Lilly (Fellowship in Diabetes and Metabolism 2005 to PI). We are grateful to the staff of the Turku PET Centre for their skilled assistance, to Jarkko Johansson for his technical support on software usage and data presentation and to Nobuyuki Kudomi for his valuable advise.

REFERENCES

[1] Quisth V, Enoksson S, Blaak E, Hagström-Toft E, Arner P, Bolinder J. Major differences in noradrenaline action on lipolysis and blood flow rates in skeletal muscle and adipose tissue *in vivo*. Diabetologia 2005; 48: 946-53.

[2] Goossens GH, Blaak EE, Saris WH, van Baak MA. Angiotensin II-induced effects on adipose and skeletal muscle tissue blood flow and lipolysis in normal-weight and obese subjects. J Clin Endocrinol Metab 2004; 89: 2690-6.

[3] Ardilouze JL, Fielding BA, Currie JM, Frayn KN, Karpe F. Nitric oxide and beta-adrenergic stimulation are major regulators of preprandial and postprandial subcutaneous adipose tissue blood flow in humans. Circulation 2004; 109: 47-52.

[4] Frayn KN, Karpe F, Fielding BA, Macdonald IA, Coppack SW. Integrative physiology of human adipose tissue. Int J Obes Relat Metab Disord 2003; 27: 875-88.

[5] Karpe F, Fielding BA, Ilic V, MacDonald IA, Summers LK, Frayn KN. Impaired Postprandial Adipose Tissue Blood Flow Response Is Related to Aspects of Insulin Sensitivity. Diabetes 2002; 51: 2467-2473.

[6] Karpe F, Tan GD. Adipose Tissue Function in the Insulin-Resistance Syndrome. Biochem Soc Trans 2005; 33: 1045-1048.

[7] Summers LK. Adipose tissue metabolism, diabetes and vascular disease--lessons from *in vivo* studies. Diab Vasc Dis Res 2006; 3: 12-21.

[8] Karpe F, Fielding BA, Ilic V, Humphreys SM, Frayn KN. Monitoring adipose tissue blood flow in man: a comparison between the (133)xenon washout method and microdialysis. Int J Obes Relat Metab Disord 2002; 26: 1-5.

[9] Ritchie SA, Connell JM. The link between abdominal obesity, metabolic syndrome and cardiovascular disease. Nutr Metab Cardiovasc Dis 2007; 17(4): 319-326.

[10] Saito T, Misawa K, Kawata S. Fatty liver and non-alcoholic steatohepatitis. Intern Med 2007; 46: 101-104.

[11] Virtanen KA, Lönnroth P, Parkkola R, *et al*. Glucose Uptake and Perfusion in Subcutaneous and Visceral Adipose Tissue during Insulin Stimulation in Nonobese and Obese Humans. J Clin Endocrinol Metab 2002; 87: 3902-3910.

[12] Naganawa M, Kimura Y, Nariai T, *et al*. Omission of serial arterial blood sampling in neuroreceptor imaging with independent component analysis. NeuroImage 2005; 26: 885-890.

[13] Naganawa M, Kimura Y, Ishii K, Oda K, Ishiwata K, Matani A. Extraction of a Plasma Time-Activity Curve From Dynamic Brain PET Images Based on Independent Component Analysis. IEEE Trans Biomed Eng 2005; 52: 201-210.

[14] Sanabria-Bohórquez SM, Maes A, Dupont P, *et al*. Image-derived Input Function for [^{11}C]Flumazenil Kinetic Analysis in Human Brain. Mol Imaging Biol 2003; 5: 72-78.

[15] Juillard L, Janier M, Fouque D, *et al*. Renal blood flow measurement by positron emission tomography using ^{15}O-labeled water. Kidney Int 2000; 57: 2511-2518.

[16] Lüdemann L, Sreenivasa G, Michel R, *et al*. Corrections of arterial input function for dynamic $H_2{}^{15}O$ PET to assess perfusion of pelvic tumours: arterial blood sampling versus image extraction. Phys Med Biol 2006; 51: 2883-2900.

[17] Germano G, Chen BC, Huang S-C, Gambhir SS, Hoffman EJ, Phelps ME. Use of the abdominal aorta for arterial input function determination in hepatic and renal PET studies. J Nucl Med 1992; 33: 613-620.

[18] Watabe H, Channing MA, Riddell C, *et al*. Noninvasive Estimation of the Aorta Input Function for Measurement of Tumor Bood Flow with [^{15}O]Water. IEEE Trans Med Imaging 2001; 20(3): 164-174.

[19] Wahl LM, Asselin M-C, Nahmias C. Regions of interest in the Venous Sinuses as Input Functions for Quantitative PET. J Nucl Med 1999; 40: 1666-1675.

[20] Chen S, Feng D. Noninvasive Quantification of the Differential Portal and Arterial Contribution to the Liver Blood Supply From PET Measurements Using the ^{11}C-Acetate Kinetic Model. IEEE Trans Biomed Eng 2004; 51: 1579-1585.

[21] Kim J, Herrero P, Sharp T, *et al.* Minimally Invasive Method of Determining Blood Input Function from PET Images in Rodents. J Nucl Med 2006; 47: 330-336.

[22] Lodge MA, Carson RE, Carrasquillo JA, Whatley M, Libutti SK, Bacharach SL. Parametric Images of Blood Flow in Oncology PET Studies Using [^{15}O]Water. J Nucl Med 2000; 41: 1784-1792.

[23] Van der Weerdt AP, Klein LJ, Boellaard R, Visser CA, Visser FC, Lammertsma AA. Image-derived Input Functions for Determination of MRGlu in Cardiac ^{18}F-FDG PET Scans. J Nucl Med 2001; 42: 1622-1629.

[24] Asselin M-C, Cunningham V, Amano S, Gunn R, Nahmias C. Parametrically defined cerebral blood vessels as non-invasive blood input functions for brain PET studies. Phys Med Biol 2004; 49: 1033-1054.

[25] Schroeder T, Vidal Melo MF, Musch G, Harris S, Venegas JG, Winkler T. Image-derived input function for assessment of ^{18}F-FDG uptake by the inflamed lung. J Nucl Med 2007; 48: 1889-96.

[26] Ruotsalainen U, Raitakari M, Nuutila P, Oikonen V, Sipilä H, Teräs M, Knuuti J, Bloomfield PM, Iida H. Quantitative blood flow measurement of skeletal muscle using oxygen-15-water and PET. J Nucl Med 1997; 38: 314-319.

[27] Meyer E. Simultaneous correction for tracer arrival delay and dispersion in CBF measurements by the $H_2{}^{15}O$ autoradiographic method and dynamic PET. J Nucl Med 1989; 30: 1069-1078.

[28] Van den Hoff J, Burchert W, Müller-Schauenburg W, Meyer G-J, Hundeshagen H. Accurate local blood flow measurements with dynamic PET: fast determination of input function delay and dispersion by multilinear minimization. J Nucl Med 1993; 34: 1770-1777.

[29] Alenius S, Ruotsalainen U. Bayesian image reconstruction for emission tomography based on median root prior. Eur J Nucl Med 1997; 24: 258-265.

[30] Press WH, Teukolsky SA, Vetterling WT, Flannery BP. Numerical Recipes in C: The Art of Scientific Computing. Cambridge University Press; 1992.

[31] Cobelli C, Forster D, Toffolo G. Tracer Kinetics in Biomedical Research: From Data to Model. Kluwer Academic Publishers; 2002.

[32] Altman D, Bland M. Measurement in Medicine: The Analysis of Method Comparison Studies. Statistician 1983; 32: 307-317.

[33] Viljanen APM, Virtanen KA, Järvisalo MJ, *et al*. Rosiglitazone treatment increases subcutaneous adipose tissue glucose uptake in parallel with perfusion in patients with type 2 diabetes: a double-blind, randomized study with metformin. J Clin Endocrinol Metab 2005; 90: 6523-6528.

[34] Virtanen KA, Peltoniemi P, Marjamäki P, *et al*. Human adipose tissue glucose uptake determined using [^{18}F]-fluoro-deoxy-glucose ([^{18}F]FDG) and PET in combination with microdialysis. Diabetologia 2001; 44: 2171-2179.

[35] Singh K, Jakobsen BK, Sohlberg S, Kumar S, Arnesen E. The difference between ultrasound and computed tomography (CT) measurements of aortic diameter increases with aortic diameter: analysis of axial images of abdominal aortic and common iliac artery diameter in normal and aneurysmal aortas: The Tromsø Study, 1994-1995. Eur J Vasc Endovasc Surg 2004; 28: 158-167.

Received: November 8, 2007 Revised: November 15, 2007 Accepted: November 21, 2007